Logarithmic profile of temperature in sheared and unstably stratified atmospheric boundary layers

Yu Cheng *
Department of Earth and Environmental Engineering, Columbia University, New York, New York 10027, USA

Qi Li
School of Civil and Environmental Engineering, Cornell University, Ithaca, New York 14853, USA

Dan Li
Department of Earth and Environment, Boston University, Boston, Massachusetts 02215, USA

Pierre Gentine
Department of Earth and Environmental Engineering and Department of Earth and Environmental Sciences, Columbia University, New York, New York 10027, USA

(Received 9 April 2020; accepted 25 February 2021; published 11 March 2021)

The impact of buoyancy on the mean velocity, temperature, and scalar concentration profiles in the lower atmosphere is typically investigated within the framework of Monin-Obukhov similarity theory (MOST). MOST is the theoretical foundation for parametrizing surface-atmosphere exchanges in nearly all weather, climate, and hydrological models. According to MOST, the classic logarithmic profiles of mean velocity and temperature break down as the buoyancy effects become important. However, recent studies on turbulent Rayleigh-Bénard convection and natural convection along vertical walls suggest that the mean temperature in the near-surface region still follows a logarithmic profile. Motivated by these new results, we study the mean potential temperature profile in sheared and unstably stratified atmospheric boundary layers using direct numerical simulations and field observations. We find that the mean potential temperature profile remains logarithmic across a wide range of stability parameters, which characterizes the relative importance of buoyancy versus shear effects. Compared to MOST, our results suggest that the buoyancy force does not modify the logarithmic nature of the mean potential temperature profile, but instead modulates its slope, which is no longer universal and differs from $1/\kappa$, where κ is the von Kármán constant. This study provides another perspective on scalar turbulence in the atmospheric boundary layer.

DOI: 10.1103/PhysRevFluids.6.034606

I. INTRODUCTION

The existence of a universal logarithmic mean velocity profile in the near-wall region of turbulent shear flows has been supported by laboratory measurements [1–3], atmospheric observations [4], and direct numerical simulations (DNSs) [5,6] following early dimensional analysis [7,8]. Similarly, the logarithmic profile for mean temperature in the near-wall region was first reported in the boundary layer over a heated flat plate in 1929 [9], and later proposed theoretically [10–12]

*yc2965@columbia.edu

and supported by DNS of channel flow [13–17] and pipe flow [18], where the flow field is free from buoyancy effects and temperature is treated as a passive scalar. However, the mean velocity [19,20] and temperature [21–24] profiles cannot be adequately described by the universal log law when buoyancy influences the flow field. To account for these buoyancy effects on the mean velocity and temperature fields, Monin-Obukhov similarity theory (MOST) [25] is often invoked.

MOST is widely used for describing the mean velocity and temperature profiles and their connections to turbulent fluxes in the atmospheric surface layer, which is located within approximately the lowest 10% of the atmospheric boundary layer (ABL) [26]. In the atmospheric surface layer, the flow is influenced by both shear and buoyancy. MOST is the theoretical foundation for formulating surface boundary conditions for numerical weather prediction [27] and climate models [28–30]. In essence, MOST [25] corrects the logarithmic profiles of mean wind, potential temperature, and scalar concentrations using stability correction functions. According to MOST, the log law for mean velocity and potential temperature gradually breaks down as the stability-dependent correction functions become more important.

However, recent work has reported logarithmic temperature profiles with varying slopes (as compared to the universal log law that has a slope of $1/\kappa$, where κ is the von Kármán constant) under different buoyant conditions in the near-wall regions of turbulent Rayleigh-Bénard convection [31–33] and natural convection along vertical walls [34]. This is at odds with the traditional paradigm in the atmospheric literature stating that the mean temperature profile in the atmospheric surface layer follows a power law under highly convective conditions [35], which can be viewed as an asymptotic state of MOST (i.e., the so-called local free convection [36]). Interestingly, the temperature log law reported by these recent studies seems to be more prevalent than the velocity log law since the former is observed in extremely buoyant flows [33] in addition to the neutral shear flows near the wall. This motivates us to examine the potential existence of a temperature log law in turbulent flows driven by both shear and buoyancy, e.g., the unstably stratified ABL.

We start by pointing out that it is well recognized that MOST does not explain all important surface-layer statistics. Notable examples include the horizontal velocity variances and spectra [37–41]. In particular, the boundary layer height z_i, not considered by MOST, has been shown to be important in describing the horizontal velocity spectra and, more importantly for our work, the temperature spectra in the atmospheric surface layer [42–44]. For instance, Tong and Ding [45] added a wave-number-dependent horizontal length scale to explain surface-layer similarity in addition to the MOST stability parameter. Therefore, it is not unreasonable to ask whether the temperature field is affected by the boundary layer height in a way that may not be captured by MOST. In particular, is there still a log law for the mean temperature profile, and if so, does the slope of the logarithmic temperature profile depend on the boundary layer height?

II. METHODS

A. Direct numerical simulations

The ABL has been studied using large eddy simulations (LESs) [46–48]. However, uncertainties exist when subgrid-scale turbulence closures are applied near the wall [49,50] and wall-modeled LESs for atmospheric studies is often based on MOST [46,51–53]. Recently, DNS has been used to study the convective ABL [23,49,54–56], which can resolve the full range of turbulence scales although the Reynolds number is smaller than that in the real atmosphere. In this study, we use five DNS experiments to study ABLs under weakly unstable, highly unstable, and free convective conditions. Key information of the five DNS experiments is summarized in Table I and more details can be found elsewhere [49,57,58].

The four simulations (named Sh40, Sh20, Sh5, and Sh2) are forced with varying mean geostrophic wind and hence have different stability conditions. For these simulations, the incompressible Navier-Stokes equations with Boussinesq approximation are solved using the code

TABLE I. Key parameters of the simulated ABLs ranging from weakly unstable conditions to free convective conditions. Re_τ is the friction Reynolds number, z_i is the boundary layer height, u_* is the friction velocity, and ν is the kinematic viscosity. L is the Obukhov length, and L_x, L_y, and L_z are the domain sizes in the x, y, and z directions, respectively. $\Delta_x^+ = (\Delta_x u_*)/\nu$, Δ_y^+ and Δ_z^+ are the spatial grid resolutions denoted by inner units in the x, y, and z directions, respectively. κ_θ is the inverse of the temperature log law slope. The range of temperature log law is also indicated using z^+, $\frac{z}{L}$, and $\frac{z}{z_i}$.

DNS data	Re_τ	$\frac{z_i}{L}$	$\frac{L_x}{L_y}$	$\frac{L_x}{L_z}$	Δ_x^+ (Δ_y^+)	Δ_z^+	κ_θ	Log-law range in z^+	Log-law range in $\frac{z}{L}$	Log-law range in $\frac{z}{z_i}$
Sh40	1900	−1.7	1	1.52	8.92	1.13	0.68	140.3–260.3	−0.23– − 0.12	0.071–0.14
Sh20	1243	−7.1	1.5	6	11.02	2.65	2.36	84.8–151.0	−0.74– − 0.44	0.062–0.10
Sh5	554	−105.1	1.5	6	4.95	1.19	12.35	36.8–67.8	−11.50– − 6.25	0.060–0.11
Sh2	309	−678.2	1.5	6	2.87	0.71	28.59	22.1–30.0	−56.57– − 41.75	0.062–0.083
Microhh ReL	80	−100171.6	1	1.87	0.19	0.21	68.68	10.0–12.0	−15153.14– − 12540.53	0.13–0.15

described in Li *et al.* [49] (for Sh2, Sh5, and Sh20) and Heerwaarden *et al.* [59] (for Sh40). A sponge layer is prescribed at the top 25% of the computational domain to prevent the reflection of gravity waves [48]. The potential temperature is initially set to increase with height in the top 50% of the computational domain to prescribe a stably stratified condition. The boundary condition for the temperature field is a constant flux at the surface and zero flux at the top of the computational domain. Periodic boundary conditions are employed in the horizontal x and y directions since the statistical properties of turbulence in the ABL are nearly homogeneous when the external forcing is uniform [46]. The grid points are $nx \times ny \times nz = 1200 \times 800 \times 602$ for the dataset Sh2, $1200 \times 800 \times 626$ for both Sh5 and Sh20, and $640 \times 640 \times 3328$ for Sh40 in streamwise (x), spanwise (y), and vertical (z) directions, respectively. The stability parameter z_i/L is −1.7, −7.1, −105.1, and −678.2 (from weakly to highly convective) for Sh40, Sh20, Sh5, and Sh2, respectively. Here z_i is the convective boundary layer height, $L = \frac{u_*^3}{\frac{\kappa g}{\Theta_r} u_* \theta_*}$ is the Obukhov length [60], u_* is the friction velocity, κ is again the von Kármán constant and is assumed to be equal to 0.4, $g = 9.81$ m^2 s^{-1} is the gravitational acceleration, Θ_r is a reference potential temperature, $\theta_* \equiv \frac{\nu_\theta}{u_*} \frac{\partial \Theta}{\partial z}_{|z=0}$ is a temperature scale, ν_θ is the thermal diffusivity, and Θ is the horizontally averaged potential temperature at height z. The friction Reynolds number $\mathrm{Re}_\tau \equiv u_* z_i/\nu = z_i/\delta_\nu$ is 1900, 1243, 554, and 309 for Sh40, Sh20, Sh5, and Sh2, respectively. Here ν is the kinematic viscosity and $\delta_\nu \equiv \nu/u_*$ is the viscous length scale.

To assess the asymptotic behavior in extremely convective conditions, we also employ another simulation of free convection (named Microhh ReL and similar to the one in Heerwaarden *et al.* [58]), which uses a constant temperature boundary condition at the surface with a stability parameter of $z_i/L = -100\,171.6$. The grid points are $nx \times ny \times nz = 1536 \times 1536 \times 768$. Heerwaarden *et al.* [58] observed Reynolds number similarity in their simulations and concluded that the DNS results may be extrapolated to higher Reynolds numbers. The selected time step for analysis in each DNS experiment is the time when the system is almost in steady state [58].

B. Field observations

The Cabauw Experimental Site for Atmospheric Research (CESAR) [61,62] (4.926° E, 51.97° N) in the Netherlands has a tower of 213 m with observations at 2, 10, 20, 40, 80, 140, and 200 m above a grass field, thus providing unique muitilevel temperature observations in the ABL. In this study we only use the data at the lowest six levels (up to 140 m). A number of 30-min data segments between 11:00 and 15:00 UTC in July 2019 are used as the raw data. These include temperature data and surface fluxes measured at 3 m, which have been quality controlled

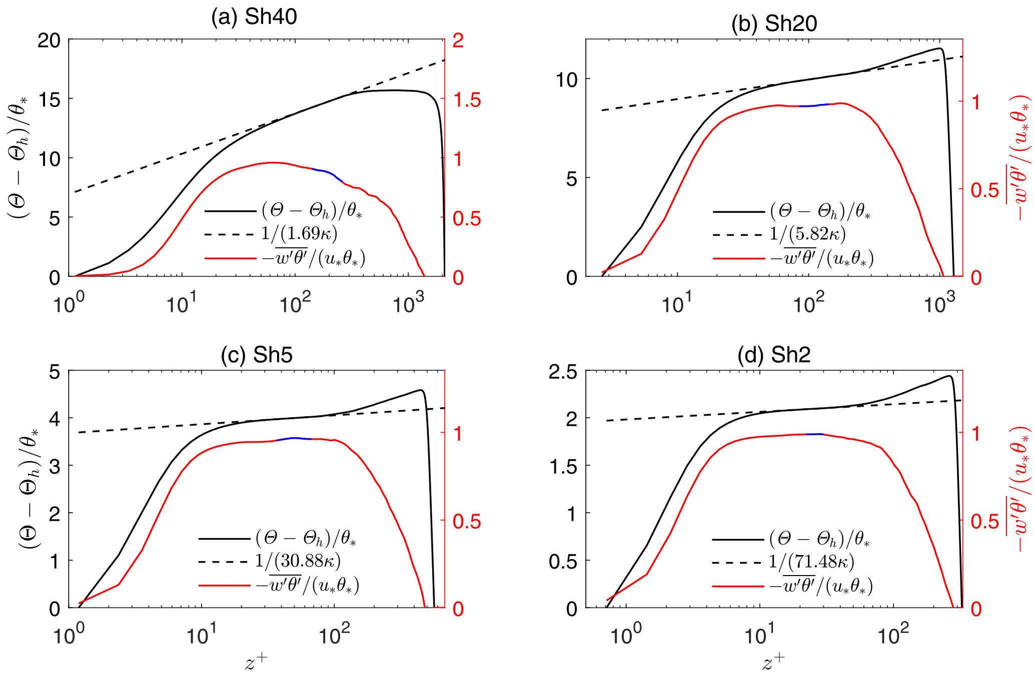

FIG. 1. Vertical profiles of normalized potential temperature and heat flux averaged in the x-y plane in different convective DNS data. w' is fluctuation of vertical velocity, θ' is fluctuation of potential temperature, and $\overline{\cdots}$ denotes averaging in the x-y plane. The black dashed line denotes the fitted log profile and the slope is shown. The blue line denotes the normalized heat flux in the log law region.

[62] and downloaded from the CESAR data archive. The boundary layer height z_i is retrieved from the Lufft CHM 15k ceilometer [63], which is used to detect the top of an elevated aerosol layer. The ceilometer backscatter profiles can be used to retrieve the ABL height as the ABL is presumably well mixed and there are significant differences between the aerosol content of the ABL and the free troposphere [64]. The average ABL height of each 30-min segment is used as the raw data.

The raw data are filtered based on two criteria: the mean scaling temperature θ_* in the 30-min sampling period has to be negative and the boundary layer height z_i is larger than 700 m. The first criterion is used to ensure that the ABL is under unstable conditions. Since we would like to include as many measurements as possible (especially those at 140 m) to cover a wide range of z, we further require that the boundary layer height z_i is large enough so that the measurements are within the atmospheric surface layer. These two criteria yield 36 different 30-min periods in July 2019.

III. RESULTS

A. Existence of a temperature log law

Similarly to Kader and Yaglom [11], the difference between the mean (horizontal average in the x-y plane) potential temperature Θ at each height z and the mean potential temperature Θ_h at the lowest DNS grid is normalized by the temperature scaling parameter θ_*. The normalized temperature $(\Theta - \Theta_h)/\theta_*$, when plotted against $z^+ \equiv z/\delta_v$, shows a logarithmic profile in certain ranges in all five DNS experiments (Fig. 1; Microhh ReL shown in Fig. S1 of the Supplemental Material [65]). Similarly to the neutral channel flow study of Lee and Moser (2015) [5], a plateau of $\frac{\kappa z}{\theta_*}\frac{\partial \Theta}{\partial z}$ is more indicative of the existence of a temperature log law (Fig. 2; Microhh ReL shown in Fig. S2 of the

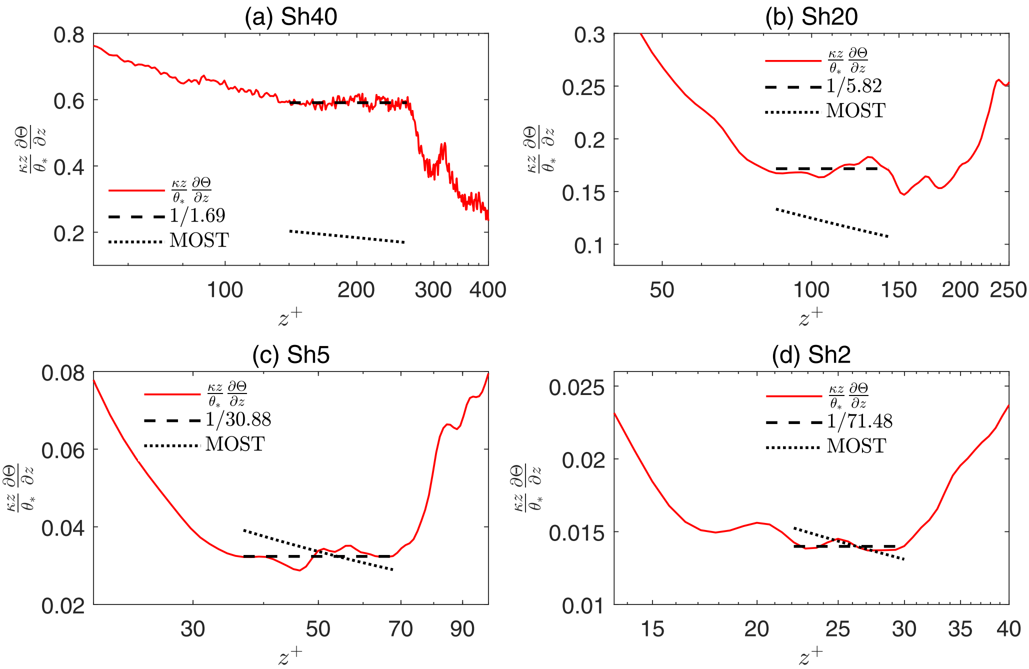

FIG. 2. The dimensionless temperature gradient $\frac{\kappa z}{\theta_*}\frac{\partial\Theta}{\partial z}$ in different DNS experiments. The black dashed line denotes the average $\frac{\kappa z}{\theta_*}\frac{\partial\Theta}{\partial z}$ in the log law region. The widely used Monin-Obukhov similarity function proposed by Businger *et al.* [67] is also shown and denoted as "MOST."

Supplemental Material). In our study, the black dashed lines (plateau) in Fig. 2 are used to denote the vertical ranges where the temperature log law exists.

Over these vertical ranges, the coefficient of determination R^2 for the relation between $(\Theta - \Theta_h)/\theta_*$ and $\ln(z^+)$ is 1.00, emphasizing their linear relation. In contrast, the normalized velocity U/u_*, where U is the mean streamwise velocity, does not follow a log law in the temperature log law ranges (details in the Supplemental Material) under more convective conditions ($R^2 \leqslant 0.22$ at $z_i/L \leqslant -105.1$). The deviation of the mean velocity profile from a log law due to buoyancy effects [20] is expected, and is also suggested by MOST. The failure to observe a velocity log law and constant momentum flux in highly convective conditions in the DNS experiments might also be related to the low Reynolds number [5]. Our finding of distinct behaviors of mean temperature and velocity is consistent with a previous study on turbulent natural convection [34].

The variations of turbulent heat flux $\overline{w'\theta'}$ (computed as $\frac{\max(\overline{w'\theta'})-\min(\overline{w'\theta'})}{\max(\overline{w'\theta'})}$) in the vertical ranges where the temperature log law exists (denoted by the blue color in Fig. 1) are 12% (Sh40), 1% (Sh20), 1% (Sh5), 0.2% (Sh2), and 0.7% (Microhh ReL), respectively. The magnitude of these variations, which is on the order of ∼1%– ∼10%, is broadly consistent with the constant-flux layer concept in the atmosphere [26]. According to Wyngaard (2010) [66], the variation of turbulent fluxes in the atmospheric surface layer should scale with the ratio of the atmospheric surface layer height to the ABL height, which is about ∼10%. Here it is noted that a constant surface heat flux is prescribed for Sh40, Sh20, Sh5, and Sh2 while a constant surface temperature is prescribed for Microhh ReL.

As detailed in Table I, the logarithmic temperature profiles are found in the range $0.06 \leqslant z/z_i \leqslant 0.14$ for Sh40 ($z_i/L = -1.7$), Sh20 ($z_i/L = -7.1$), Sh5 ($z_i/L = -105.1$), and Sh2 ($z_i/L = -678.2$). This is again consistent with the typical ratio of the atmospheric surface layer height to the ABL height (∼10%) [26]. We note that the temperature log law range in terms of z^+ is very different for

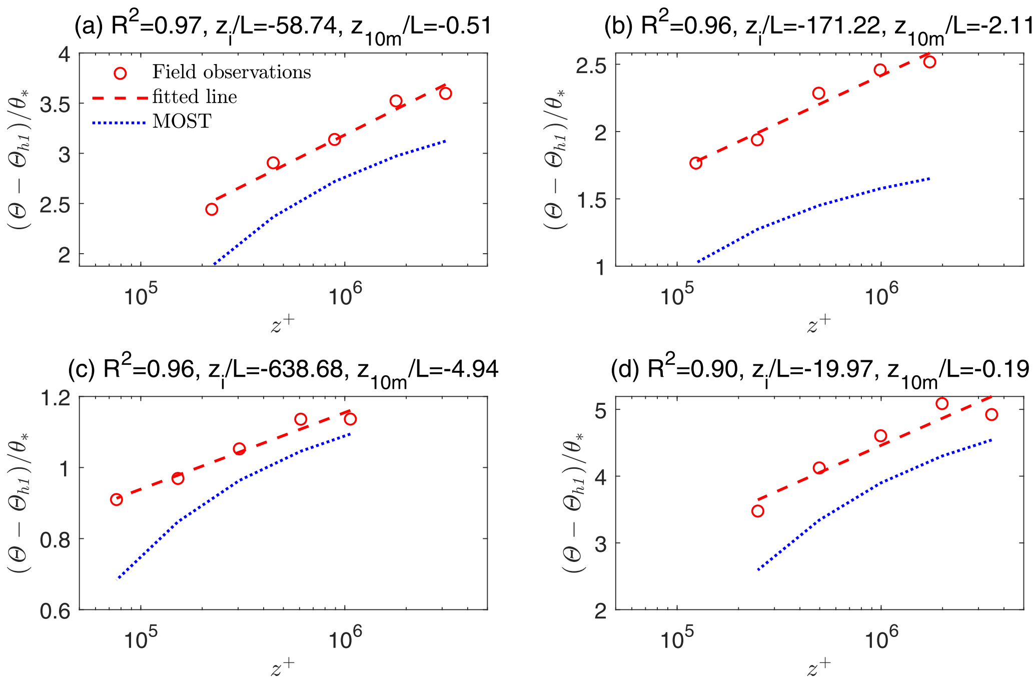

FIG. 3. Vertical profiles of normalized potential temperature in four different unstable conditions at the Cabauw Experimental Site for Atmospheric Research in the Netherlands. R^2 denotes the coefficient of determination for the relation between $\frac{\Theta-\Theta_{h1}}{\theta_*}$ and $\ln(z^+)$, and z_{10m}/L denotes the stability parameter z/L at $z = 10$ m. "MOST" denotes the computed temperature profiles based on Monin-Obukhov similarity theory.

different DNS experiments, which implies some Reynolds-number dependence. The temperature log law range for the least buoyant DNS experiment Sh40 ($Re_\tau = 1900$, $z_i/L = -1.7$) is $140.3 \leqslant z^+ \leqslant 260.3$, which compares well with the velocity log law range $3{Re_\tau}^{1/2} < z^+ < 0.15Re_\tau$ (corresponding to $131 < z^+ < 285$ when $Re_\tau = 1900$) in turbulent shear flows according to Marusic *et al.* [3]. Importantly, using the MOST stability parameter, the temperature log law is found to exist even when $z/L < -10$ (e.g., in Sh2 which has $z/L \approx -50$). This is surprising as MOST would have predicted that the mean temperature profile deviates strongly from the log law under such conditions [see Fig. 2(d)]. This highlights the fundamental difference between our results and MOST.

The slope of the temperature log law is not constant but instead decreases from $1/(1.69\kappa)$ to $1/(71.48\kappa)$ when z_i/L decreases from -1.7 to -678.2 (Fig. 1). This is in contrast with the universal log law for mean velocity in turbulent shear flows which has a constant slope of $1/\kappa$ [3]. Such variations of the temperature log law slope have been also observed in studies of turbulent Rayleigh-Bénard convection [31]. We will examine the variation of the temperature log law slope later.

The field observations at the Cabauw Experimental Site for Atmospheric Research are at much higher Reynolds numbers ($9.8 \times 10^6 \leqslant Re_\tau \leqslant 3.7 \times 10^7$). The normalized potential temperature $(\Theta - \Theta_{h1})/\theta_*$ is plotted against $\ln(z^+)$ in all 36 periods (Fig. 3 and Figs. S3– S6 in the Supplemental Material), where Θ is the time-averaged potential temperature at heights of 10, 20, 40, 80, and 140 m above the land surface in a 30-min period, and Θ_{h1} is the time-averaged potential temperature at 2 m in the same period. θ_* is computed using turbulent fluxes measured at 3 m assuming that the measurements are taken in the constant-flux layer. One can see that $(\Theta - \Theta_{h1})/\theta_*$ seems to show a linear relation with $\ln(z^+)$ over a wide range of stability conditions as compared to the nonlinear relation due to MOST, suggesting that the mean temperature profile follows a log law. When we fit a linear relation between $(\Theta - \Theta_{h1})/\theta_*$ and $\ln(z^+)$, the coefficient of determination is higher than

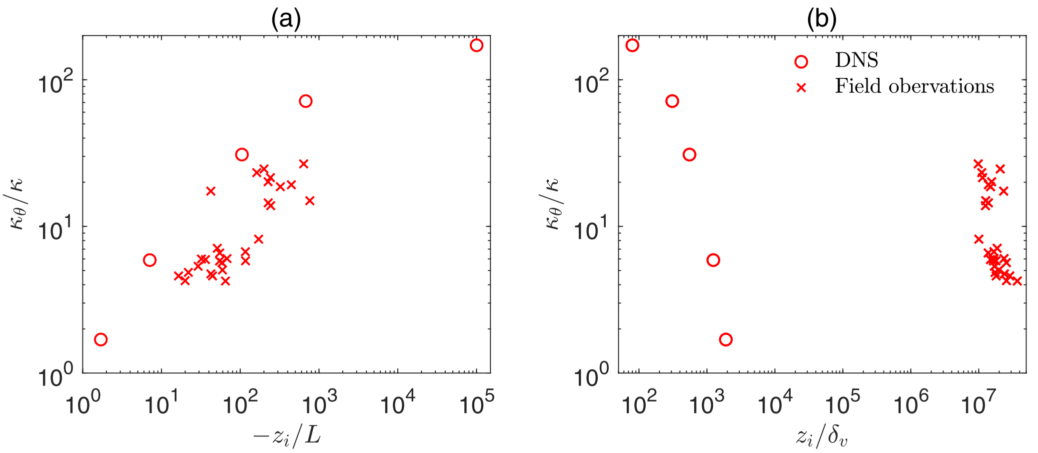

FIG. 4. The ratio κ_θ/κ plotted against $-z_i/L$ (a), and z_i/δ_v (b) in various convective DNS datasets and field observations.

0.7 in 29 of the 36 periods. We also compare the predicted temperature profile based on MOST [68,69] with field observations and find deviations across the stability conditions examined here ($-5.22 \leqslant z/L \leqslant -0.19$, where $z = 10$ m) (Fig. 3). We note that the coefficient of determination is lower than 0.7 in 7 of the 36 periods, where there are also significant deviations from MOST (Fig. S6 in the Supplemental Material). This might be due to measurement uncertainties, thus these seven periods are not further used to compute the slope of the temperature log law (Fig. 4).

We point out that there have been few studies investigating the logarithmic nature of the mean potential temperature profile in the atmospheric surface layer. This is partly because field observations typically have very sparse vertical measurements (fewer than those used in our study) that do not permit one to validate the logarithmic behavior in the surface layer. As a result of the sparse measurements in the vertical direction and the large measurement uncertainties, a plateau of $\frac{\kappa z}{\theta_*}\frac{\partial \Theta}{\partial z}$ cannot be accurately identified in order to support a log law in field observations. In addition, MOST has been regarded as a cornerstone of ABL turbulence theory and thus most field studies analyzed data within the framework of MOST assuming its validity. Nonetheless, we highlight that previous field observations showed that the peak wave numbers of temperature spectra are related to z_i [42,43], suggesting that the temperature profiles might be also influenced by z_i, as shown in our results.

B. Slope of the temperature log law

1. Dimensional analysis

In this section, the slope of the temperature log law is analyzed using dimensional analysis. The mean temperature profile in fully developed unstable boundary layer flows can be described by ν, z_i, u_τ, z, and θ_*, which can form three nondimensional groups: $\frac{z}{z_i}$, $\frac{z_i}{\delta_v} \equiv \mathrm{Re}_\tau$, and $\frac{z_i}{L} = \frac{\kappa g \theta_*}{\Theta_r}\frac{z_i}{u_*^2}$. The mean temperature distribution can be written as $\Theta_0 - \Theta = \theta_* F_0(\frac{z}{z_i}, \frac{z_i}{\delta_v}, \frac{z_i}{L})$, where Θ_0 is mean potential temperature at the wall, and F_0 is a function of $\frac{z}{z_i}$, $\frac{z_i}{\delta_v}$, and $\frac{z_i}{L}$. In the log law region, $\frac{\kappa z}{\theta_*}\frac{\partial \Theta}{\partial z}$ is independent of z as suggested by the DNS datasets, which is fundamentally different from the z-dependence profile according to MOST (Fig. 2). Similarly to the argument for velocity gradient in Pope [70], the temperature gradient $\frac{\partial \Theta}{\partial z}$ can be written as

$$\frac{\partial \Theta}{\partial z} = \frac{\theta_*}{z}\Phi\left(\frac{z_i}{\delta_v}, \frac{z_i}{L}\right), \tag{1}$$

where Φ is a function of $\frac{z_i}{\delta_v}$ and $\frac{z_i}{L}$. Integrating from a reference height z_r to z and denoting $\frac{1}{\kappa_\theta} \equiv \Phi(\frac{z_i}{\delta_v}, \frac{z_i}{L})$ yield

$$\frac{\Theta - \Theta_r}{\theta_*} = \frac{1}{\kappa_\theta} \ln\left(\frac{z}{z_r}\right), \tag{2}$$

where Θ_r is a reference potential temperature at some reference height z_r near the wall. We can normalize both z and z_r by δ_v to recast the equation in terms of $z^+ = z/\delta_v$ but this will not affect the slope $1/\kappa_\theta$, which is a function of z_i/L and z_i/δ_v. z_i/L represents the buoyancy effects and z_i/δ_v represents the Reynolds number effects. This dimensional analysis points out the relevant parameters that affect the slope of the temperature log law, but the exact relations remain to be determined from numerical experiments or field observations.

2. DNS and field observations

The DNS datasets (Sh40, Sh20, Sh5, Sh2, and Microhh ReL) suggest that κ_θ/κ increases nonlinearly with increasing $-z_i/L$ [Fig. 4(a)]. That is to say, as buoyancy effects increase, the slope of the temperature log law deviates more from that of the neutral turbulent shear flow. In the Sh40 experiment ($-z_i/L = -1.7$) with the weakest buoyancy effects, $\kappa_\theta/\kappa = 1.69$, thus we expect that κ_θ/κ approaches 1 in the "neutral limit" without buoyancy effects assuming that the turbulent Prandtl number in the neutral limit is equal to 1 [71,72]. It is worth noting that κ_θ/κ may still depend on the Reynolds number in the "neutral limit", which is consistent with the dependence of temperature profiles on the Reynolds number in previous DNS experiments neglecting buoyancy effects [13–18]. In the "free convection limit", κ_θ/κ might further increase with increasing $-z_i/L$ but the increasing rate is not as large as that in less buoyant conditions [Fig. 4(a)]. Consistent with the DNS datasets, κ_θ/κ increases with increasing $-z_i/L$ in field observations [Fig. 4(a)]. In terms of the dependence on the Reynolds number, the DNS datasets suggest that κ_θ/κ seems to decrease with increasing z_i/δ_v [Fig. 4(b)]. However, when z_i/δ_v increases from $\sim 10^3$ (DNS datasets) to $\sim 10^7$ (field observations), κ_θ/κ does not seem to show a monotonic trend [Fig. 4(b)], and one may argue that κ_θ/κ becomes nearly independent of z_i/δ_v in field observations.

Therefore, it can be summarized that κ_θ/κ is mainly determined by $-z_i/L$, but also influenced by z_i/δ_v when the Reynolds number is not sufficiently large. In Fig. 4(a), κ_θ/κ obtained from field observations seems to be smaller than those from DNS experiments at similar $-z_i/L$, which might be due to the Reynolds number effects as discussed above and/or uncertainties in field observations of turbulent fluxes [73] and the ABL height [74,75]. More accurate measurements of mean temperature gradients in the ABL, turbulent fluxes, and the ABL height are critical to better constrain κ_θ in atmospheric conditions with large Reynolds numbers. We leave this for further study.

3. Asymptotic analysis

As κ_θ seems to become independent of the Reynolds number when the Reynolds number is sufficiently high in field observations [Fig. 4(b)] similarly to the von Kármán constant κ [3], we conduct asymptotic analysis for the slope κ_θ in the "neutral limit" and "free convection limit" at sufficiently high Reynolds numbers (i.e., neglecting the Reynolds number effects). In the neutral limit ($\theta_* \to 0$ and $z_i/L \to 0$), we obtain the following asymptotic state:

$$\Phi\left(\frac{z_i}{\delta_v}, \frac{z_i}{L}\right) = \Phi\left(\frac{z_i}{L}\right) = \Phi(0) = c_1, \quad \text{for } \frac{z_i}{L} \to 0, \tag{3}$$

where c_1 is a constant. Given that $\kappa_\theta = 1/\Phi$, we thus expect

$$\kappa_\theta = \frac{1}{c_1}, \quad \text{for } \frac{z_i}{L} \to 0. \tag{4}$$

Note that $c_1 = 1/\kappa$ if we further assume that the turbulent Prandtl number in the neutral limit is equal to 1 [71,72].

If the proposed temperature log law [Eq. (1) or (2)] holds in the free convection limit ($\theta_* \to -\infty$ and $z_i/L \to -\infty$), the following asymptotic relation is required to cancel out θ_*:

$$\Phi\left(\frac{z_i}{\delta_v}, \frac{z_i}{L}\right) = \Phi\left(\frac{z_i}{L}\right) = \Phi\left(\frac{\kappa g z_i}{\Theta_r}\frac{\theta_*}{u_*^2}\right) = c_2\left(-\frac{\kappa g z_i}{\Theta_r}\frac{\theta_*}{u_*^2}\right)^{-1}, \quad \text{for } \frac{z_i}{L} \to -\infty, \tag{5}$$

where c_2 is a constant. Under such conditions, the temperature gradient $\partial\Theta/\partial z$ can then be rewritten as

$$\frac{\partial\Theta}{\partial z} = -c_2\frac{\Theta_r}{z}\frac{u_*^2}{\kappa g z_i}, \quad \text{for } \frac{z_i}{L} \to -\infty. \tag{6}$$

The above equation can accommodate the situation of $u_* \to 0$ as it corresponds to a well-mixed state (i.e., $\partial\Theta/\partial z = 0$). Furthermore, because $\kappa_\theta = 1/\Phi$, we can obtain

$$\kappa_\theta = \frac{1}{c_2}\left(-\frac{z_i}{L}\right), \quad \text{for } \frac{z_i}{L} \to -\infty. \tag{7}$$

This asymptotic behavior of κ_θ is in qualitative but not quantitative agreement with the relation between κ_θ and $-z_i/L$ obtained from the DNS experiments and field observations, where the slope between κ_θ and $-z_i/L$ in the log-log plot is smaller than unity [Fig. 4(a)]. The limited Reynolds number as well as the limited buoyancy may influence the relationship between κ_θ and $-z_i/L$. On the one hand, the DNS experiments have low Reynolds numbers. On the other hand, the free convection limit ($z_i/L \to -\infty$) may not be reached in field observations ($z_i/L > -1000$), which also suffer from measurement uncertainties.

C. Comparison to MOST

The proposed temperature log law in unstable boundary layers can be written as

$$\frac{\kappa z}{\theta_*}\frac{\partial\Theta}{\partial z} = \kappa\Phi\left(\frac{z_i}{L}, \frac{z_i}{\delta_v}\right) = \frac{\kappa}{\kappa_\theta}, \tag{8}$$

where $\Phi(\frac{z_i}{L}, \frac{z_i}{\delta_v})$ is independent of z. This is fundamentally different from MOST where the normalized temperature gradient is assumed to depend on z/L [25],

$$\frac{\kappa z}{\theta_*}\frac{\partial\Theta}{\partial z} = \phi_h\left(\frac{z}{L}\right). \tag{9}$$

The fact that ϕ_h is dependent on the distance to the wall z leads to a nonlogarithmic profile for the mean temperature. The widely used Businger-Dyer function for ϕ_h [67] is shown in Fig. 2, which clearly denotes a slope rather than a plateau for $\frac{\kappa z}{\theta_*}\frac{\partial\Theta}{\partial z}$. In our DNS datasets, $\frac{\kappa z}{\theta_*}\frac{\partial\Theta}{\partial z}$ approaches a constant that is equal to $\frac{\kappa}{\kappa_\theta}$ in the surface layer (Figs. 2 and S2), thus supporting a log law rather than MOST. Moreover, the proposed log layer depends on an outer layer scaling, the boundary height z_i. This outer layer correction, $\Phi(\frac{z_i}{L}, \frac{z_i}{\delta_v})$, is consistent with recent studies emphasizing the importance of z_i in the temperature spectra [42,43], heat-flux cospectra [43], and temperature profiles [41,49] in convective conditions. Yet, the role of z_i is not considered in MOST.

IV. CONCLUSION

We investigate the existence of a logarithmic potential temperature profile in the near-wall region of unstable boundary layer flows using DNS experiments and field observations. The new temperature log law can be expressed as $\frac{\kappa_\theta z}{\theta_*}\frac{\partial\Theta}{\partial z} = 1$, where κ_θ is a function of z_i/L and z_i/δ_v, which represent the buoyancy and Reynolds number effects, respectively. The proposed temperature log law is fundamentally different from the traditional MOST and thus would alter our representation of flux boundary conditions in hydrological and atmospheric models. We also conduct asymptotic analysis for the slope κ_θ in the "neutral limit" and "free convection limit" at sufficiently high

Reynolds numbers. Further investigations using more data collected over a wide range of stability and Reynolds number conditions are recommended. With more validations, the proposed temperature log law may replace Monin-Obukhov similarity function in weather and climate models and wall models for LES, potentially leading to better predictions of weather, climate, and hydrology.

ACKNOWLEDGMENTS

P.G. would like to acknowledge funding from the National Science Foundation (NSF CAREER, EAR-1552304) and from the Department of Energy (DOE Early Career, DE-SC00142013). Q.L. acknowledges funding from the National Science Foundation (AGS-2028644, CBET-2028842). D.L. acknowledges funding support from the National Science Foundation (AGS-1853354). The simulations were performed on the computing clusters of the National Center of Atmospheric Research under projects UCLB0017 and UCOR00029. We would like to thank Dr. Chiel van Heerwaarden for the help with direct numerical simulation of free convection using MicroHH. We would like to thank Dr. Fred C. Bosveld and Henk Klein Baltink for the help in obtaining the field data at the Cabauw Experimental Site for Atmospheric Research (Cesar) [76].

[1] B. J. Mckeon, J.-d. Li, W. Jiang, J. F. Morrison, and A. J. Smits, Further observations on the mean velocity distribution in fully developed pipe flow, J. Fluid Mech. **501**, 135 (2004).

[2] P. A. Monkewitz, K. A. Chauhan, and H. M. Nagib, Self-consistent high-Reynolds-number asymptotics for zero-pressure-gradient turbulent boundary layers, Phys. Fluids **19**, 115101 (2007).

[3] I. Marusic, J. P. Monty, M. Hultmark, and A. J. Smits, On the logarithmic region in wall turbulence, J. Fluid Mech. **716**, R3 (2013).

[4] E. L. Andreas, K. J. Claffey, R. E. Jordan, C. W. Fairall, P. S. Guest, P. O. G. Persson, and A. A. Grachev, Evaluations of the von Kármán constant in the atmospheric surface layer, J. Fluid Mech. **559**, 117 (2006).

[5] M. Lee and R. D. Moser, Direct numerical simulation of turbulent channel flow up to $\mathrm{Re}_\tau \approx 5200$, J. Fluid Mech. **774**, 395 (2015).

[6] Y. Yamamoto and Y. Tsuji, Numerical evidence of logarithmic regions in channel flow at $\mathrm{Re}_\tau = 8000$, Phys. Rev. Fluids **3**, 012602(R) (2018).

[7] T. von Karman, Mechanische ähnlichkeit und turbulenz, Nachr. Ges. Wiss. Göttingen, Math.-Phys. Klasse (1930), 58–76.

[8] C. B. Millikan, A critical discussion of turbulent flow in channels and circular tubes, in *Proceedings of the Fifth International Congress on Applied Mechanics (Cambridge, MA, 1938)* (Wiley, New York, 1938), pp. 386–392.

[9] F. Éliás, Die wärmeübertragung einer geheizten platte an strömende luft. I. Anlage und ergebnisse der versuche, Z. Angew. Math. Mech. **9**, 434 (1929).

[10] L. D. Landau and E. M. Lifshitz, *Course of Theoretical Physics: Vol. 6 Fluid Mechanics* (Pergamon, New York, 1959).

[11] B. Kader and A. Yaglom, Heat and mass transfer laws for fully turbulent wall flows, Int. J. Heat Mass Transfer **15**, 2329 (1972).

[12] B. Kader, Temperature and concentration profiles in fully turbulent boundary layers, Int. J. Heat Mass Transfer **24**, 1541 (1981).

[13] J. Kim and P. Moin, Transport of passive scalars in a turbulent channel flow, *Turbulent Shear Flows 6* (Springer, New York, 1989), pp. 85–96.

[14] N. Kasagi, Y. Tomita, and A. Kuroda, Direct numerical simulation of passive scalar field in a turbulent channel flow, J. Heat Transfer **114**, 598 (1992).

[15] H. Kawamura, H. Abe, and Y. Matsuo, DNS of turbulent heat transfer in channel flow with respect to Reynolds and Prandtl number effects, Int. J. Heat Fluid Flow **20**, 196 (1999).

[16] H. Abe, H. Kawamura, and Y. Matsuo, Surface heat-flux fluctuations in a turbulent channel flow up to $\mathrm{Re}_\tau = 1020$ with $\mathrm{Pr} = 0.025$ and 0.71, Int. J. Heat Fluid Flow **25**, 404 (2004).

[17] H. Abe and R. A. Antonia, Relationship between the heat transfer law and the scalar dissipation function in a turbulent channel flow, J. Fluid Mech. **830**, 300 (2017).

[18] L. Redjem-Saad, M. Ould-Rouiss, and G. Lauriat, Direct numerical simulation of turbulent heat transfer in pipe flows: Effect of Prandtl number, Int. J. Heat Fluid Flow **28**, 847 (2007).

[19] O. Iida and N. Kasagi, Direct numerical simulation of unstably stratified turbulent channel flow, J. Heat Transfer **119**, 53 (1997).

[20] A. Scagliarini, H. Einarsson, Á. Gylfason, and F. Toschi, Law of the wall in an unstably stratified turbulent channel flow, J. Fluid Mech. **781**, R5 (2015).

[21] A. Garai, J. Kleissl, and S. Sarkar, Flow and heat transfer in convectively unstable turbulent channel flow with solid-wall heat conduction, J. Fluid Mech. **757**, 57 (2014).

[22] S. Sid, Y. Dubief, and V. Terrapon, Direct numerical simulation of mixed convection in turbulent channel flow: On the Reynolds number dependency of momentum and heat transfer under unstable stratification, in *Proceedings of the Eighth International Conference on Computational Heat and Mass Transfer (ICCHMT 2015)* (2015).

[23] S. Pirozzoli, M. Bernardini, R. Verzicco, and P. Orlandi, Mixed convection in turbulent channels with unstable stratification, J. Fluid Mech. **821**, 482 (2017).

[24] D. Li, K. Luo, and J. Fan, Buoyancy effects in an unstably stratified turbulent boundary layer flow, Phys. Fluids **29**, 015104 (2017).

[25] A. Monin and A. Obukhov, Basic laws of turbulent mixing in the ground layer of the atmosphere, Tr. Geofiz. Inst. Akad. Nauk. SSSR **151**, 163 (1954).

[26] R. B. Stull, *An Introduction to Boundary Layer Meteorology* (Springer Science & Business Media, Berlin, 1988), Vol. 13.

[27] J.-F. Louis, A parametric model of vertical eddy fluxes in the atmosphere, Bound.-Layer Meteorol. **17**, 187 (1979).

[28] J. W. Deardorff, Parameterization of the planetary boundary layer for use in general circulation models, Mon. Weather Rev. **100**, 93 (1972).

[29] I. Troen and L. Mahrt, A simple model of the atmospheric boundary layer; sensitivity to surface evaporation, Bound.-Layer Meteorol. **37**, 129 (1986).

[30] A. Holtslag and B. Boville, Local versus nonlocal boundary-layer diffusion in a global climate model, J. Clim. **6**, 1825 (1993).

[31] G. Ahlers, E. Bodenschatz, D. Funfschilling, S. Grossmann, X. He, D. Lohse, R. J. A. M. Stevens, and R. Verzicco, Logarithmic Temperature Profiles in Turbulent Rayleigh-Bénard Convection, Phys. Rev. Lett. **109**, 114501 (2012).

[32] S. Grossmann and D. Lohse, Logarithmic temperature profiles in the ultimate regime of thermal convection, Phys. Fluids **24**, 125103 (2012).

[33] G. Ahlers, E. Bodenschatz, and X. He, Logarithmic temperature profiles of turbulent Rayleigh–Bénard convection in the classical and ultimate state for a Prandtl number of 0.8, J. Fluid Mech. **758**, 436 (2014).

[34] M. Hölling and H. Herwig, Asymptotic analysis of the near-wall region of turbulent natural convection flows, J. Fluid Mech. **541**, 383 (2005).

[35] C. Priestley, Convection from a large horizontal surface, Aust. J. Phys. **7**, 176 (1954).

[36] J. Wyngaard, O. Coté, and Y. Izumi, Local free convection, similarity, and the budgets of shear stress and heat flux, J. Atmos. Sci. **28**, 1171 (1971).

[37] J. C. Kaimal, J. Wyngaard, Y. Izumi, and O. Coté, Spectral characteristics of surface-layer turbulence, Q. J. R. Meteorol. Soc. **98**, 563 (1972).

[38] J. Kaimal, Horizontal velocity spectra in an unstable surface layer, J. Atmos. Sci. **35**, 18 (1978).

[39] S. Caughey and S. Palmer, Some aspects of turbulence structure through the depth of the convective boundary layer, Q. J. R. Meteorol. Soc. **105**, 811 (1979).

[40] H. A. Panofsky, H. Tennekes, D. H. Lenschow, and J. Wyngaard, The characteristics of turbulent velocity components in the surface layer under convective conditions, Bound.-Layer Meteorol. **11**, 355 (1977).

[41] C. Johansson, A.-S. Smedman, U. Högström, J. G. Brasseur, and S. Khanna, Critical test of the validity of Monin–Obukhov similarity during convective conditions, J. Atmos. Sci. **58**, 1549 (2001).

[42] K. McNaughton, R. Clement, and J. Moncrieff, Scaling properties of velocity and temperature spectra above the surface friction layer in a convective atmospheric boundary layer, Nonlinear Process. Geophys. **14**, 257 (2007).

[43] J. Laubach and K. G. McNaughton, Scaling properties of temperature spectra and heat-flux cospectra in the surface friction layer beneath an unstable outer layer, Bound.-Layer Meteorol. **133**, 219 (2009).

[44] D. Li, G. Katul, and P. Gentine, The k^{-1} scaling of air temperature spectra in atmospheric surface layer flows, Q. J. R. Meteorol. Soc. **142**, 496 (2016).

[45] C. Tong and M. Ding, Multi-point Monin–Obukhov similarity in the convective atmospheric surface layer using matched asymptotic expansions, J. Fluid Mech. **864**, 640 (2019).

[46] C.-H. Moeng, A large-eddy-simulation model for the study of planetary boundary-layer turbulence, J. Atmos. Sci. **41**, 2052 (1984).

[47] J. W. Deardorff, Numerical investigation of neutral and unstable planetary boundary layers, J. Atmos. Sci. **29**, 91 (1972).

[48] F. T. Nieuwstadt, P. J. Mason, C.-H. Moeng, and U. Schumann, Large-eddy simulation of the convective boundary layer: A comparison of four computer codes, *Turbulent Shear Flows 8* (Springer, New York, 1993), pp. 343–367.

[49] Q. Li, P. Gentine, J. P. Mellado, and K. A. McColl, Implications of nonlocal transport and conditionally averaged statistics on Monin–Obukhov similarity theory and Townsend's attached eddy hypothesis, J. Atmos. Sci. **75**, 3403 (2018).

[50] J.-P. Mellado, C. Bretherton, B. Stevens, and M. Wyant, DNS and LES for simulating stratocumulus: Better together, J. Adv. Model. Earth Syst. **10**, 1421 (2018).

[51] S. Khanna and J. G. Brasseur, Analysis of Monin–Obukhov similarity from large-eddy simulation, J. Fluid Mech. **345**, 251 (1997).

[52] E. Bou-Zeid, C. Meneveau, and M. Parlange, A scale-dependent Lagrangian dynamic model for large eddy simulation of complex turbulent flows, Phys. Fluids **17**, 025105 (2005).

[53] H. Schmidt and U. Schumann, Coherent structure of the convective boundary layer derived from large-eddy simulations, J. Fluid Mech. **200**, 511 (1989).

[54] J. P. Mellado, C. C. van Heerwaarden, and J. R. Garcia, Near-surface effects of free atmosphere stratification in free convection, Bound.-Layer Meteorol. **159**, 69 (2016).

[55] K. Fodor, J. P. Mellado, and M. Wilczek, On the role of large-scale updrafts and downdrafts in deviations from Monin–Obukhov similarity theory in free convection, Bound.-Layer Meteorol. **172**, 371 (2019).

[56] A. Haghshenas and J. P. Mellado, Characterization of wind-shear effects on entrainment in a convective boundary layer, J. Fluid Mech. **858**, 145 (2019).

[57] Y. Cheng, M. Giometto, P. Kauffmann, L. Lin, C. Cao, C. Zupnick, H. Li, Q. Li, R. Abernathey, and P. Gentine, Deep learning for subgrid-scale turbulence modeling in large-eddy simulations of the atmospheric boundary layer, arXiv:1910.12125.

[58] C. C. v. Heerwaarden, V. Stratum, and J. P. Mellado, Growth and decay of a convective boundary layer over a surface with a constant temperature, J. Atmos. Sci. **73**, 2165 (2016).

[59] C. C. v. Heerwaarden, B. J. Van Stratum, T. Heus, J. A. Gibbs, E. Fedorovich, and J. P. Mellado, MicroHH 1.0: A computational fluid dynamics code for direct numerical simulation and large-eddy simulation of atmospheric boundary layer flows, Geosci. Model Dev. **10**, 3145 (2017).

[60] A. Obukhov, Turbulence in thermally inhomogeneous atmosphere, Trudy Inst. Teor. Geofiz. Akad. Nauk SSSR **1**, 95 (1946).

[61] A. Apituley, H. Russchenberg, H. van der Marel, F. Bosveld, R. Boers, H. ten Brink, G. de Leeuw, R. Uijlenhoet, B. Arbresser-Rastburg, and T. Rockmann, Overview of research and networking with ground based remote sensing for atmospheric profiling at the Cabauw Experimental Site for Atmospheric Research (CESAR)–the Netherlands, in *IGARSS 2008-2008 IEEE International Geoscience and Remote Sensing Symposium*, Vol. 3 (IEEE, New York, 2008), pp. III–903.

[62] F. C. Bosveld, P. Baas, A. C. Beljaars, A. A. Holtslag, J. V.-G. de Arellano, and B. J. Van De Wiel, Fifty years of atmospheric boundary-layer research at Cabauw serving weather, air quality and climate, Bound.-Layer Meteorol. **177**, 583 (2020).

[63] L. Choma, T. Musil, H. Némethová, J. Jevčák, P. Petríček, S. Makó, M. Pilát, and F. Balla, Comparative analysis of selected ceilometers for practice and academic purposes, in *2019 Modern Safety Technologies in Transportation (MOSATT)* (IEEE, New York, 2019), pp. 35–38.

[64] M. d. Bruine, A. Apituley, D. P. Donovan, H. Klein Baltink, and M. J. d. Haij, Pathfinder: Applying graph theory to consistent tracking of daytime mixed layer height with backscatter lidar, Atmos. Meas. Tech. **10**, 1893 (2017).

[65] See Supplemental Material at http://link.aps.org/supplemental/10.1103/PhysRevFluids.6.034606 for temperature profiles of the free convection numerical experiment and field observations, and velocity profiles of numerical experiments.

[66] J. C. Wyngaard, *Turbulence in the Atmosphere* (Cambridge University Press, Cambridge, UK, 2010).

[67] J. A. Businger, J. C. Wyngaard, Y. Izumi, and E. F. Bradley, Flux-profile relationships in the atmospheric surface layer, J. Atmos. Sci. **28**, 181 (1971).

[68] H. A. Panofsky, Determination of stress from wind and temperature measurements, Q. J. R. Meteorol. Soc. **89**, 85 (1963).

[69] G. Kramm, D. J. Amaya, T. Foken, and N. Mölders, Hans A. Panofsky's integral similarity function—At fifty, Atmos. Clim. Sci. **3**, 581 (2013).

[70] S. Pope, *Turbulent Flows* (Cambridge University Press, Cambridge, UK, 2000).

[71] D. Li, G. G. Katul, and S. S. Zilitinkevich, Revisiting the turbulent Prandtl number in an idealized atmospheric surface layer, J. Atmos. Sci. **72**, 2394 (2015).

[72] D. Li, Turbulent Prandtl number in the atmospheric boundary layer—Where are we now? Atmos. Res. **216**, 86 (2019).

[73] D. E. Reed, J. M. Frank, B. E. Ewers, and A. R. Desai, Time dependency of eddy covariance site energy balance, Agric. For. Meteorol. **249**, 467 (2018).

[74] P. Seibert, F. Beyrich, S.-E. Gryning, S. Joffre, A. Rasmussen, and P. Tercier, Review and intercomparison of operational methods for the determination of the mixing height, Atmos. Environ. **34**, 1001 (2000).

[75] S. Pal, M. Haeffelin, and E. Batchvarova, Exploring a geophysical process-based attribution technique for the determination of the atmospheric boundary layer depth using aerosol lidar and near-surface meteorological measurements, J. Geophys. Res. Atmos. **118**, 9277 (2013).

[76] http://www.cesar-database.nl.